AIP | Applied Physics Letters

High-resolution wide-field Raman imaging through a fiber bundle

Lyubov V. Doronina-Amitonova, Il'ya V. Fedotov, Andrey B. Fedotov, and Aleksei M. Zheltikov

Citation: Appl. Phys. Lett. **102**, 161113 (2013); doi: 10.1063/1.4801847
View online: http://dx.doi.org/10.1063/1.4801847
View Table of Contents: http://apl.aip.org/resource/1/APPLAB/v102/i16
Published by the American Institute of Physics.

High-resolution wide-field Raman imaging through a fiber bundle

Lyubov V. Doronina-Amitonova,[1,2,3] Il'ya V. Fedotov,[1,2,3] Andrey B. Fedotov,[1,2,3] and Aleksei M. Zheltikov[1,2,3,4,5]
[1]*Physics Department, International Laser Center, M. V. Lomonosov Moscow State University, Moscow 119992, Russia*
[2]*Russian Quantum Center, ul. Novaya 100, Skolkovo, Moscow Region 1430125, Russia*
[3]*Kurchatov Institute National Research Center, Moscow, Russia*
[4]*Department of Physics and Astronomy, Texas A&M University, College Station, Texas 77843-4242, USA*
[5]*Center of Photochemistry, Russian Academy of Sciences, ul. Novatorov 7a, Moscow 117421, Russia*

(Received 1 March 2013; accepted 1 April 2013; published online 25 April 2013)

Wide-field Raman imaging with a spatial resolution of a few micrometers is demonstrated using bundles of thousands of hexagonally packed optical fibers. Raman images are synthesized pixel by pixel, by sequentially coupling the laser pump into individual fibers of the bundle with a galvanometric scanner and collecting the Raman response from the laser-excited region of the sample within the entire aperture of the distal end of the same fiber bundle. © *2013 AIP Publishing LLC*. [http://dx.doi.org/10.1063/1.4801847]

The Raman effect offers a broad variety of powerful analytical tools for spectroscopic studies[1] and species-selective imaging within a broad class of physical, chemical, and biological systems.[2] Over the past years, the Raman instrumentation and methodology have been constantly progressing toward meeting the challenges of real-life applications, including *in vivo* studies in biology,[3] standoff detection of potential biohazard contaminants, air pollution, and explosives,[4] monitoring of DNA synthesis,[5] as well as chemically specific detection of signatures of pathologies and diseases in medicine.[6] For many of these applications, it is critical that the studies be performed in the endoscopic or remote-detection mode. This strongly motivates the search for fiber solutions for the Raman studies. A variety of fiber probes have been demonstrated for fiber-based Raman spectroscopy,[2,5,7,8] helping optimize signal collection and discriminate the Raman signal from the sample against the Raman background from the fiber. The search for optimal fiber probes for Raman imaging is, however, still ongoing. Arrays of optical fibers have been shown[2,9] to enable fast processing of Raman images collected with imaging optics, such as microscope objectives. Raman chemical imaging with submillimeter spatial resolution has been demonstrated[10] with a fiberscope where fiber-optic components for beam delivery are spatially separated from the light-collecting fiber bundle and are integrated with spectral filters. Multicore fibers with integrated fiber Bragg gratings have been shown to offer much promise for background-free Raman sensing[11] as well as for diagnosis and screening of cancerous tissues.[12]

Here, we demonstrate wide-field Raman imaging with a spatial resolution of a few micrometers using bundles of several thousands of hexagonally packed optical fibers. Raman images are synthesized in our scheme pixel by pixel, by sequentially coupling the laser pump into individual fibers of the bundle with a galvanometric scanner and collecting the Raman response from the laser-excited region of the sample within the entire aperture of the distal end of the same fiber bundle.

Our method of fiber Raman imaging is based on a fiber-bundle microprobe coupled to a computer-controlled galvanometric scanner[13] and a system for Raman signal detection (Fig. 1). Fiber bundles of different types were used in our experiments, with the number of fibers in a hexagonal array within the bundle (Fig. 2(a)) varying from several tens to several thousands. The diameter d of individual fibers in these fiber bundles ranged from 1.0 to 2.4 μm, with the distance Λ between the centers of individual fibers in the bundles varying from 3.0 to 11 μm. A typical field of view provided by our fiber-bundle microprobe about 0.07 mm^2 for a bundle with an outer diameter of 300 μm.

The pump beam, provided by the second-harmonic output of a continuous-wave Nd:YAG laser with a wavelength $\lambda \approx 532$ nm, is coupled into the individual fibers in the fiber bundle through a 40×, NA = 0.65 objective with two galvanometric mirrors (Fig. 1), orthogonally scanning the laser beams over the input end of the fiber bundle with a minimum step of 0.5 μm.

The laser pump transmitted through the fiber bundle induces a Raman response from a laser-irradiated area of a sample. This Raman signal is collected by the entire aperture of the same fiber bundle and is transmitted to the input end of the bundle, toward the detection system. Following beam collimation with a system of lenses, a targeted Raman signal is selected from the spectrum of the signal transmitted through the fiber and detected with a photomultiplier (Fig. 1). Raman imaging are synthesized in our scheme pixel by pixel, by repeating this measurements for all the fibers in the bundle.

Experiments with two types of Raman samples were performed to demonstrate Raman imaging through a fiber bundle. One series of experiments was aimed at imaging surface defects and imperfections on polystyrene films. In another series of experiments, clusters of diamond nanoparticles on a glass substrate were studied. Diamond and polystyrene were chosen for our experiments as they provide representative examples of Raman-active systems with distinctly different frequency separation of their Raman modes from the Raman band of silica, leading to radically different signal-to-background ratios in fiber-based Raman imaging.

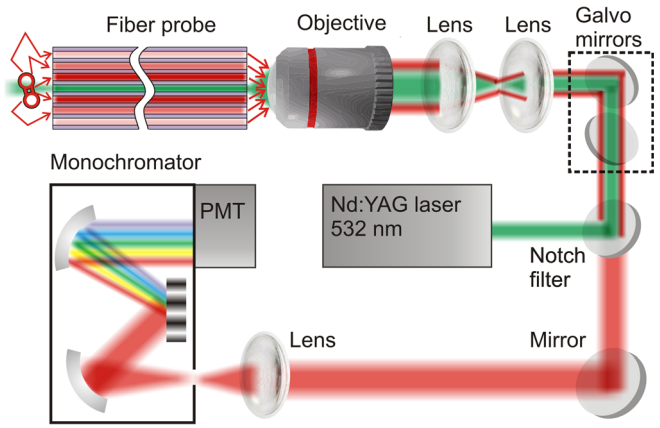

FIG. 1. Raman imaging through a fiber bundle.

In Fig. 2(b), panoramic Raman spectra of a polystyrene film (curve 1) and clusters of diamond nanoparticles on a glass substrate (curve 2) are shown against the Raman spectrum of the fiber bundle used in our experiments (curve 3). All these spectra were measured with the second-harmonic output of a continuous-wave Nd:YAG laser used as a pump. The Raman spectrum of diamond nanoparticles is dominated by the Raman response of the zone-center $\Gamma^{(25+)}$ (F_{2g}) symmetry optical phonon at $\Omega_d \approx 1330\,\mathrm{cm}^{-1}$. This peak is only slightly detuned off the high-frequency edge of the Raman band of fused silica, observed at 1200–1250 cm^{-1}. The Raman peak of the CH stretch vibration mode of polystyrene, on the other hand, is observed in the spectral region (centered at $\Omega_p \approx 3050\,\mathrm{cm}^{-1}$), where the Raman signal from silica is very weak (cf. curves 1 and 3 in Fig. 2(b)), enabling high-contrast spectral discrimination of the Raman response of the CH stretch vibration mode against the Raman background from the fiber probe.

Typical Raman images taken through a fiber-bundle microprobe with $d \approx 2.4\,\mu\mathrm{m}$ and $\Lambda \approx 3\,\mu\mathrm{m}$ are presented in Figs. 3–5. With the laser pump beam scanned across the input end of the fiber bundle with a step of 0.5 μm, the image elements corresponding to a single measurement performed with the laser pump delivered to the sample through one of the fibers of the bundle appear as well-resolved dots in the Raman images (Figs. 3(a), 4(a)–4(d)). The spatial resolution of Raman imaging in this scheme is defined by the distance Λ between the centers of individual fibers in the fiber bundle and is estimated as 3 μm for the images shown in Figs. 3(a)–4(b).

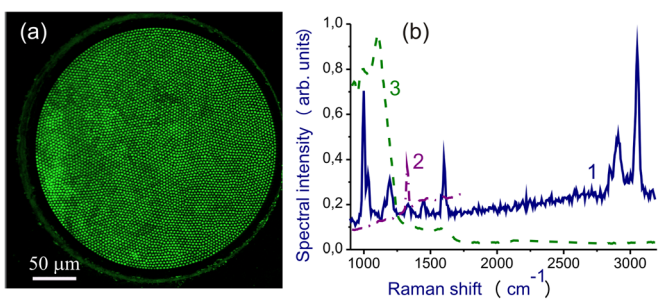

FIG. 2. (a) Cross-sectional view of a fiber-bundle microprobe with hexagonally packed fibers. The scale bar is 50 μm. (b) Panoramic Raman spectra of (1) a polystyrene film, (2) clusters of diamond nanoparticles on a glass substrate, and (3) fiber-bundle microprobe measured with the second-harmonic output of a continuous-wave Nd:YAG laser used as a pump.

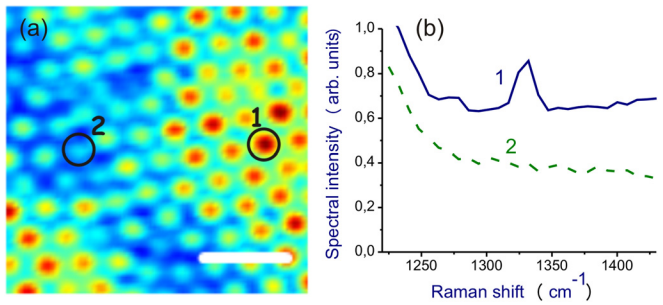

FIG. 3. (a) An image of clusters of diamond nanoparticles randomly distributed over a glass substrate measured with a fiber-bundle microprobe with $d \approx 2.4\,\mu\mathrm{m}$ and $\Lambda \approx 3\,\mu\mathrm{m}$ and a monochromator adjusted to transmit the signal within a spectral window corresponding to Raman shifts from 1220 to 1430 cm^{-1}. (b) The Raman spectra measured through fibers labeled as 1 (curve 1) and 2 (curve 2) in the image of Fig. 3(a). The scale bar is 10 μm.

In Fig. 3(a), we present an image of clusters of diamond nanoparticles randomly distributed over a glass substrate measured with a monochromator slit adjusted to transmit the signal within a spectral window corresponding to Raman shifts from 1220 to 1430 cm^{-1}. Curves 1 and 2 in Fig. 3(b) show the Raman spectra measured with the laser pump delivered through fibers seen as pixels labeled as 1 and 2 in the image of Fig. 3(a). The laser pump delivered through fiber 1 hits a cluster of diamond nanoparticles, giving rise to a Raman signal from the optical-phonon mode of diamond with a prominent peak at $\Omega_d \approx 1330\,\mathrm{cm}^{-1}$ in the Raman spectra (curve 1 in Fig. 3(b)). The laser pump transmitted through fiber 2, on the other hand, misses out diamond clusters, producing only the background signal due to Raman scattering in the fiber (curve 2 in Fig. 3(b)).

Figure 4 presents the Raman images of clusters of diamond nanoparticles on a glass substrate taken through the same fiber bundle microprobe with the monochromator set to transmit only the signal within a 10 cm^{-1} spectral window centered at the Raman shift $\Omega_d = 1330\,\mathrm{cm}^{-1}$. The Raman image in Fig. 4(a) visualizes a circular agglomeration of nanodiamond clusters on a glass substrate, while Fig. 4(b) presents an image of diamond nanoparticles randomly distributed over a glass substrate with a letter-A-shaped raised relief, whose contour is clearly seen as a dark field in the image.

The Raman signal from the CH stretch mode of polystyrene, as can be seen from the spectra presented in

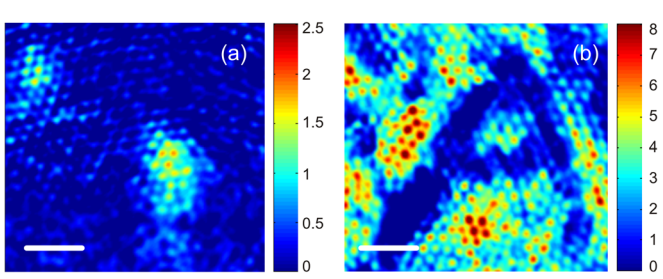

FIG. 4. Images of (a) a circular agglomeration of nanodiamond clusters on a glass substrate and (b) diamond nanoparticles randomly distributed over a glass substrate with a letter-A-shaped raised relief. The images are taken through a fiber-bundle microprobe with $d \approx 2.4\,\mu\mathrm{m}$ and $\Lambda \approx 3\,\mu\mathrm{m}$ and a monochromator adjusted to transmit only the signal within a 10-cm^{-1} spectral window centered at $\Omega_d = 1330\,\mathrm{cm}^{-1}$. The scale bar is 20 μm.

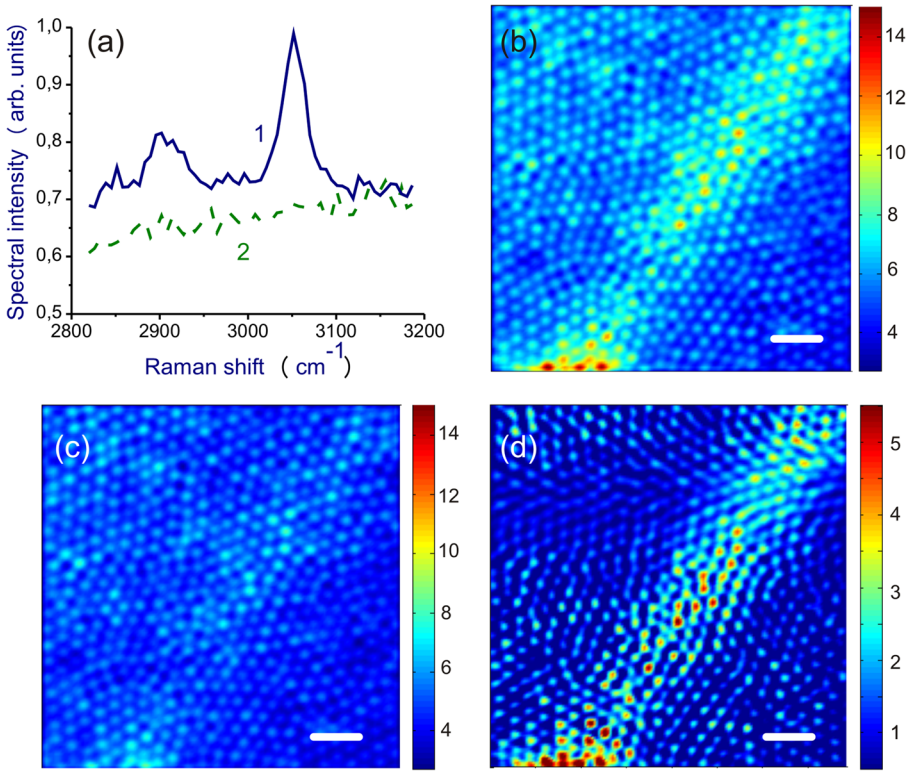

FIG. 5. (a) The Raman spectra measured through the fiber bundle with (curve 1) and without (curve 2) a polystyrene sample. (b) and (c) An image of a ridge on a polystyrene film taken through the fiber bundle microprobe with the monochromator adjusted to transmit only the signal within a 10-cm^{-1} spectral window centered at (b) 3050 cm^{-1} and (c) 3000 cm^{-1}. (d) An image following the subtraction of the background due to Raman scattering in the fiber. The scale bar is 10 μm.

Figs. 2(b) and 5(a), provides an even higher contrast of the Raman signal measured through the fiber bundle as the frequency of this mode (curve 1 in Fig. 2(b)) lies further off the high-frequency edge of the Raman band of fused silica (curve 3 in Fig. 2(b)), translating into a higher ratio of the Raman signal from the 3050 cm^{-1} CH stretch mode of polystyrene (curve 1 in Fig. 5(a)) relative to the Raman background from the fiber (curve 2 in Fig. 5(a)). In Fig. 5(b), we present an image of a 15-μm-wide ridge on a polystyrene film taken through the fiber bundle microprobe with the monochromator adjusted to transmit only the signal within a 10-cm^{-1} spectral window centered at $\Omega_p = 3050\,\text{cm}^{-1}$. The contrast of this image is limited by the background signal from the fiber and can be enhanced through background subtraction. To this end, a background signal distribution is measured (Fig. 5(c)) for the fiber bundle with the 10 cm^{-1} spectral window of the monochromator centered at 3000 cm^{-1}, i.e., tuned off the 3050 cm^{-1} Raman mode of polystyrene. Subtraction of this background from the Raman image of Fig. 5(b) yields a high-contrast Raman image of the ridge on the surface of a polystyrene film (Fig. 5(d)). Well-isolated pixels, especially clearly seen in the images after background subtraction (Fig. 5(d)), represent individual fibers in the bundle, suggesting that a resolution at the level of 1 μm can be achieved with this approach to Raman imaging by using fiber bundles with $\Lambda \approx 1\,\mu$m, which is certainly within the reach of modern fiber-optic technologies.

To summarize, we have demonstrated wide-field Raman imaging with a spatial resolution of a few micrometers using bundles of several thousands of hexagonally packed optical fibers. Raman images are synthesized in our scheme pixel by pixel, by sequentially coupling the laser pump into individual fibers of the bundle with a galvanometric scanner and collecting the Raman response from the laser-excited region of the sample within the entire aperture of the distal end of the same fiber bundle.

We are grateful to Professor K. V. Anokhin for illuminating discussions, encouragement, and valuable help. This work was supported in part by the Russian Foundation for Basic Research, the Welch Foundation (Grant No. A-1801), and Skolkovo Foundation (Grant No. 78).

[1]*Practical Raman Spectroscopy*, edited by D. J. Gardiner and P. R. Graves (Springer, Berlin, 1989).
[2]S. Stewart, R. J. Priore, M. P. Nelson, and P. J. Treado, Annu. Rev. Anal. Chem. **5**, 337 (2012).
[3]C. Krafft, B. Dietzek, and J. Popp, Analyst **134**, 1046 (2009).
[4]A. Tripathi, E. D. Emmons, P. G. Wilcox, J. A. Guicheteau, and D. K. Emge, Appl. Spectrosc. **65**, 611 (2011).
[5]L. V. Doronina-Amitonova, I. V. Fedotov, A. B. Fedotov, K. V. Anokhin, M.-L. Hu, C.-Y. Wang, and A. M. Zheltikov, Opt. Lett. **37**, 4642 (2012).
[6]C. Otto, J. de Grauw, and J. Duindam, J. Raman Spectrosc. **28**, 143 (1997).
[7]R. L. McCreery, M. Fleischmann, and P. Hendra, Anal. Chem. **55**, 146 (1983).
[8]J. T. Motz, M. Hunter, L. H. Galindo, J. A. Gardecki, J. R. Kramer, R. R. Dasari, and M. S. Feld, Appl. Opt. **43**, 542 (2004).
[9]J. Ma and D. Ben-Amotz, Appl. Spectrosc. **51**, 1845 (1997).
[10]P. J. Treado, M. P. Nelson, S. A. Keitzer, and R. D. Smith, U.S. Patent 6,788,860 B1 (7 September 2004).
[11]S. Dochow, I. Latka, M. Becker, R. Spittel, J. Kobelke, K. Schuster, A. Graf, S. Brückner, S. Unger, M. Rothhardt, B. Dietzek, C. Krafft, and J. Popp, Opt. Express **20**, 20156 (2012).
[12]C. Krafft, S. Dochow, I. Latka, B. Dietzek, and J. Popp, Biomed. Spectrosc. Imaging **1**, 39–55 (2012).
[13]L. V. Doronina-Amitonova, I. V. Fedotov, O. Efimova, M. Chernysheva, A. B. Fedotov, K. V. Anokhin, and A. M. Zheltikov, Appl. Phys. Lett. **101**, 233702 (2012).